


Developments in the Ni–Nb–Zr amorphous alloy membranes

A review

S. Sarker¹ · D. Chandra¹  · M. Hirscher² · M. Dolan³ · D. Isheim⁴ ·
J. Wermer⁵ · D. Viano³ · M. Baricco⁶ · T. J. Udovic⁷ · D. Grant⁸ ·
O. Palumbo⁹ · A. Paolone⁹ · R. Cantelli¹⁰

Received: 5 November 2015 / Accepted: 20 January 2016
© Springer-Verlag Berlin Heidelberg 2016

Abstract Most of the global H₂ production is derived from hydrocarbon-based fuels, and efficient H₂/CO₂ separation is necessary to deliver a high-purity H₂ product. Hydrogen-selective alloy membranes are emerging as a viable alternative to traditional pressure swing adsorption processes as a means for H₂/CO₂ separation. These membranes can be formed from a wide range of alloys, and those based on Pd are the closest to commercial deployment. The high cost of Pd (USD ~31,000 kg⁻¹) is driving the development of less-expensive alternatives, including inexpensive amorphous (Ni₆₀Nb₄₀)_{100-x}Zr_x alloys. Amorphous alloy membranes can be fabricated directly from the

molten state into continuous ribbons via melt spinning and depending on the composition can exhibit relatively high hydrogen permeability between 473 and 673 K. Here we review recent developments in these low-cost membrane materials, especially with respect to permeation behavior, electrical transport properties, and understanding of local atomic order. To further understand the nature of these solids, atom probe tomography has been performed, revealing amorphous Nb-rich and Zr-rich clusters embedded in majority Ni matrix whose compositions deviated from the nominal overall composition of the membrane.

✉ D. Chandra
dchandra@unr.edu

¹ Materials Science and Engineering, University of Nevada, MS 388, Reno, NV 89557, USA

² Max-Planck-Institut für Intelligente Systeme, Heisenbergstrasse 3, 70569 Stuttgart, Germany

³ CSIRO, QCAT, Energy, 1 Technology Court, Pullenvale, QLD 4069, Australia

⁴ Materials Science and Engineering, Northwestern University, 2220 N. Campus Dr., Evanston, IL 60208, USA

⁵ Los Alamos National Laboratory, Los Alamos, NM 875451, USA

⁶ Department of Chemistry and NIS, University of Turin, Via P. Giura, 9, 10125 Turin, Italy

⁷ National Institute of Standards and Technology, Gaithersburg, MD 20899, USA

⁸ University of Nottingham, University Park, Nottingham NG7 2RD, UK

⁹ CNR-ISC, U.O.S. La Sapienza, Piazzale A. Moro 5, 00185 Rome, Italy

¹⁰ University of Rome, La Sapienza, 00185 Roma, Italy

1 Introduction

The bulk of global H₂ production still originates from the conversion of hydrocarbon fuels such as coal, crude oil, natural gas, and biomass, and the co-production of CO₂ necessitates a H₂/CO₂ separation process to deliver H₂ of the desired purity to downstream processes [1, 2]. Pressure swing adsorption (PSA) is a reliable, established technique for this separation, but is less than ideal from an efficiency and size perspective. Alloy membranes offer the advantage of compact size and continuous separation, but are currently limited to small-scale, niche applications. For example, crystalline Pd and Pd–Ag (100–200 μm thickness) membranes have been employed for several decades to obtain ultrapure H₂ [3–9]. The reported hydrogen selectivity and permeability of these membranes vary widely, but H₂ flux values in excess of 1 mol m⁻² s⁻¹ have been reported [10]. A limitation of Pd-based membranes is the potential for hydride formation under certain operating conditions, and this can lead to eventual failure of the membrane because of increased brittleness. The greatest barrier to further deployment of Pd membrane technology

is the high price of Pd metal: In recent times, the cost of Pd has risen from USD 160 oz⁻¹ in April 2003 to USD 697 oz⁻¹ in September 2015. This cost is driving the development of less-expensive alternative membrane materials. Steward's [11] review of hydrogen permeability showed several metals have equivalent or greater permeability than Pd. Furthermore, many of these metals, such as Ni, Co, Nb, and Zr, cost in the range of USD 1–3 oz⁻¹, making them of great interest as potential Pd-alternatives.

In particular, amorphous alloys formed from a combination of Ni and one or more early transition metals (ETMs) show great promise for this application. Amorphous alloy membranes are formed directly from the molten state via a technique known as melt spinning, in which the molten alloy is rapidly solidified on the surface of a rolling copper wheel, acting as heat sink. Cooling rates as fast as 10⁵ K s⁻¹ can be achieved by this method and typically produce continuous ribbons, typically 20–60 μm thick and ca. 25 mm wide.

One of the main barriers to the use of amorphous membranes is their propensity to crystallize during long-term operation at elevated temperatures, a process which increases atomic density and leads to reduction in hydrogen diffusion pathways. In addition, crystallization often induces brittleness in the ribbon, limiting as a consequence the operating conditions. In this review, we explore this phenomenon further by presenting studies that have been performed on Ni–Nb–Zr amorphous membrane alloys regarding permeation; electrical, chemical homogeneity and local atomic order; and electrical and mechanical properties.

2 Brief history of the development of amorphous alloy membranes

The very first amorphous AuSi alloy was prepared at the California Institute of Technology in 1960 by Klement et al. [12]. Since then, significant research advances were made on understanding the nature of membranes in Japan, particularly at the Tohoku University and AIST. The amorphous membranes are generally fabricated by melt spinning methods, with critical cooling rates >10⁵ K s⁻¹. In the late 1980s, Inoue et al. [13] and Inoue [14] discovered glass-forming ability and formation of bulk metallic glasses (BMG) in La–Al–Ni and La–Al–Cu by casting in copper molds at relatively slow cooling rates <100 K s⁻¹. Inoue et al. [13] also established important parameters for the formation of BMG in which three or more components are needed with atomic size ratio >12 %, and a negative heat of mixing. The selection of compositions for metallic glass formation can be driven by thermodynamic arguments [15], and metallic glasses with various compositions

have been produced. The BMG multicomponent alloys are used for structural and other applications, whereas thin amorphous alloys discussed in this paper are mainly used in magnetic applications and membranes for hydrogen separation.

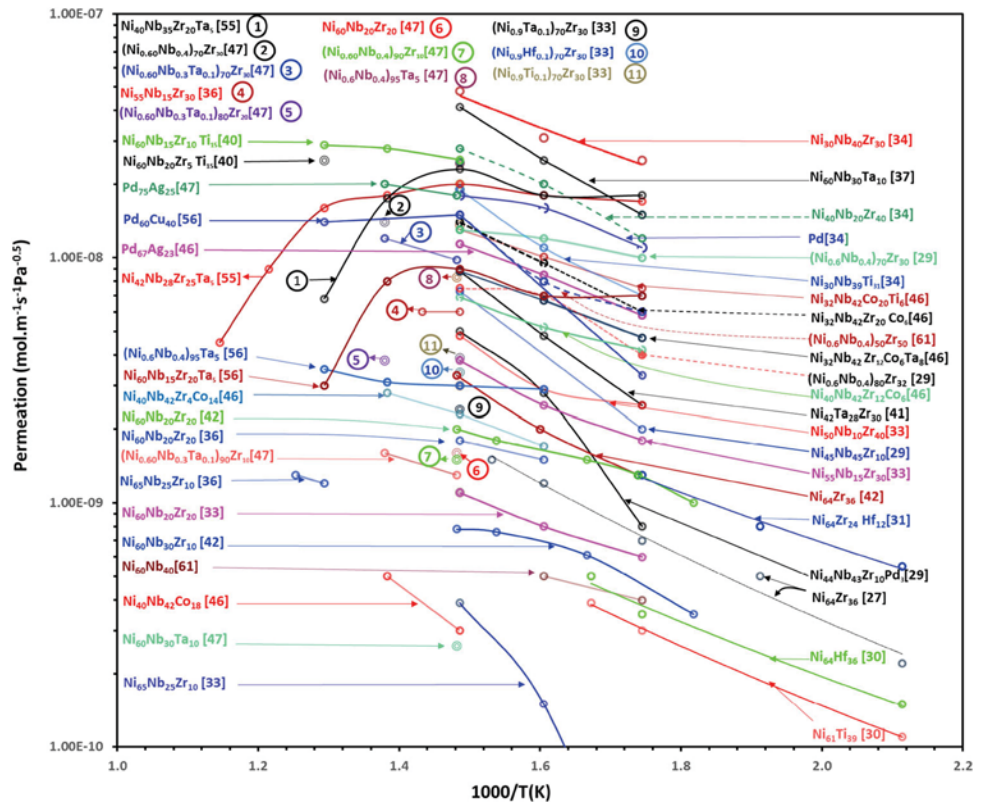
Several membrane types can be employed for the separation of H₂ from CO₂, namely ceramic ion transport membranes, inorganic microporous membranes, and alloy membranes, both crystalline and amorphous. Several notable reviews on these various membrane technologies have been published. In 2006, Phair and Donelson [16] reviewed developments in non-palladium alloy membranes related to design and preparation of alloys for hydrogen permeability, and critical performance features of Ti, Zr, Hf, and the V/Nb/Ta group of elements and alloys. In the same year, Phair and Badwal [17] reviewed materials for separation of membranes for hydrogen and oxygen production, H₂ and CO₂ separation, and power generation, and Dolan et al. [18] published a comprehensive review on hydrogen-selective amorphous membranes. They reported on significant issues related to amorphous membranes with respect to crystallization during long-term sustainability of amorphous membranes at elevated temperatures (673 K). They also discussed factors affecting diffusion rates, influence of hydrogen on thermal stability site symmetry and energies. In 2007 Ockwig and Nenoff [19] reviewed different types of hydrogen separation membranes and reported hydrogen permeabilities of NiAl, VAl, VNiAl, NbMo, NbPd, NbTiNi, VTi, VCo, Zr–Ti–Ni, and other alloys, in a temperature range of 475–673 K and VCrTi from 793 to 923 K.

The exploration of hydrogen absorption properties of Ni-based amorphous alloys started in 1981. Spit et al. [20] and Aoki et al. [21] both presented hydrogen absorption properties of amorphous Ni–Zr alloys. More hydrogen separation membranes were developed in the 1990s such as Pd_{73.2}Si₁₈M_{8.8} (M = Ag, Cu, Cr, Fe, Ni), Ni₆₀Zr₄₀, and other alloys [22–26]. The pioneering work on permeation through the Ni-based amorphous alloys was first reported by Hara et al. [27] in 2000, who produced melt spun ribbons of Ni₆₄Zr₃₆ for separation of hydrogen from CO₂. They found permeation rates >1 × 10⁻⁹ mol m⁻¹ s⁻¹ Pa^{-0.5} yielding high-purity H₂, without need for a catalytic Pd overlay.

3 Amorphous Ni-based membranes

The Ni–Nb–Zr alloy system is the most widely studied from the perspective of hydrogen separation. A summary plot of hydrogen permeation through Ni–Nb–Zr alloys, with alloying elements such as Ta, Co, Hf, and others, is shown in Fig. 1; selected crystalline Pd-based alloys are

Fig. 1 Summary of reported hydrogen permeability values for Ni-based amorphous alloy membranes and selected Pd-based alloys as reference materials



included as reference. Please note that single data points found in the literature appear as double circled symbols in this figure. In general, the permeation rates of Ni–Nb–Zr membranes are approximately in the range of 5×10^{-8} and $1 \times 10^{-10} \text{ mol m}^{-1} \text{ s}^{-1} \text{ Pa}^{-0.5}$. Also note that the alloys from reference 34 in Fig. 1 are crystalline.

The addition of Nb to Ni–Zr alloys brings the beneficial effects of increased crystallization temperature and fracture strength [28, and reduced susceptibility to hydrogen embrittlement [29]. Kimura et al. [28] produced wide, high-quality, amorphous Ni–Nb–Zr melt spun ribbons of $(\text{Ni}_{0.50}\text{Nb}_{0.50})_{100-x}\text{Zr}_x$, where $x = 10, 20, 30, 40$, and $\text{Ni}_{60}\text{Nb}_{40-x}\text{Zr}_x$, where $x = 10, 20, 30, 40$, and measured thermal and mechanical properties, but did not report any permeation results.

In 2003, Yamaura et al. [29] investigated hydrogen permeation membranes of $(\text{Ni}_{0.60}\text{Nb}_{0.40})_{100-x}\text{Zr}_x$ ($x = 0\text{--}40 \text{ at.}\%$) and showed comparable permeation rates with Pd and Pd–Ag at temperatures of 573–673 K. Also, in 2003, Hara et al. [30] explored the possibility of making ribbons of Ni–Zr with Ti and Hf additions and found that the permeabilities of Ni–Zr alloys decreased with the addition of Ti or Hf due to increased activation energies. Hara et al. [30] continued studies on $\text{Zr}_{36-x}\text{Hf}_x\text{Ni}_{64}$ ($0 \leq x \leq 36$) and observed that the ribbons did crack during tests that lasted for a few days in the temperature range of 473–623 K, but reported that the

hydrogen solubility parameters closely followed Sieverts’ law [31].

Yamaura et al. [32] studied formabilities of ribbons and performed exhaustive work by adding different alloying elements to a $(\text{Ni}_{0.60}\text{Nb}_{0.40})_{45}\text{Zr}_{50}\text{M}_5$ master alloy, where $\text{M} = \text{Ti, Ta, Sn, Si, Pd, Cu, Co, and Al}$, and reported relatively high permeation rates. The permeabilities of Cu and Co are reported as 2.34×10^{-8} and $2.46 \times 10^{-8} \text{ mol m}^{-1} \text{ s}^{-1} \text{ Pa}^{-0.5}$ at 673 K, respectively [32]; these values are as high as those of well-known conventional Pd–23 %Ag alloys, which have a permeation rate of $\sim 1.0 \times 10^{-8} \text{ (mol m}^{-1} \text{ s}^{-1} \text{ Pa}^{-0.5})$ at 673 K [29]. They also found that the addition of alloying elements like Cu, Co, Pd, Al, and P to the amorphous alloy ribbon of $(\text{Ni}_{0.6}\text{Nb}_{0.4})_{50}\text{Zr}_{50}$ increased the Vickers hardness (VH) 460, 500, 510, 510, and 560 Hv, respectively. This resulted in the decrease of permeability as a function of increased VH [32]. The permeability with the addition of amphoteric element P ($2.5 \times 10^{-8} \text{ mol m}^{-1} \text{ s}^{-1} \text{ Pa}^{-0.5}$) was found to be the lowest. One possible explanation of this is inhomogeneity in the atomic configurations resulting from higher negative mixing enthalpy of Zr–P atomic pairs as compared to the other pairs of Ni–P and Nb–P, which may have increased the hardness of the alloy. The heat of mixing of Ni–P = 26 kJ/mol of Ni, Nb–P = –81 kJ/mol of Nb, Zr–P = –119 kJ/mol of Zr, whereas pairing of Ni, Nb, and Zr atoms with Cu in the $(\text{Ni}_{0.6}\text{Nb}_{0.4})_{50}\text{Zr}_{50}$

amorphous alloy show the following mixing enthalpies: Ni–Cu = +4 kJ/mol of Ni, Nb–Cu = +3 kJ/mol of Nb, Zr–Cu = –23 kJ/mol of Zr, suggesting less segregation and lower hardness, leading greater permeability [32].

Yamaura et al. [33] continued their studies on permeation rates of the ternary alloy series $(\text{Ni}_{0.60}\text{M}_{0.40})_{70}\text{Zr}_{30}$ ($\text{M} = \text{Ti}, \text{Nb}, \text{Hf}$), $(\text{Ni}_{0.90}\text{M}_{0.10})_{70}\text{Zr}_{30}$ ($\text{M} = \text{Y}, \text{Hf}, \text{Ti}, \text{Nb}, \text{Ta}$), and $\text{Ni}_{70-x/2}\text{Nb}_{30-x/2}\text{Zr}_x$ ($x = 10\text{--}60$) and reported that addition of Nb improves hydrogen permeability. In one case, cast eutectic crystalline $\text{Ni}_{30}\text{Nb}_{40}\text{Zr}_{30}$, $\text{Ni}_{40}\text{Nb}_{20}\text{Zr}_{40}$, and $\text{Ni}_{30}\text{Nb}_{39}\text{Ti}_{31}$ alloy thick disks made by Ishikawa et al. [34] for hydrogen permeation were surprisingly reported to have 2.9 times greater permeability than that of pure Pd.

Cobalt has been explored as an alloying addition to Ni–Nb–Zr alloys by several groups. Shimpo et al. [35] investigated Co additions to the melt spun amorphous Ni–Nb–Zr alloys and measured the permeability of $(\text{Ni}_{0.60}\text{Nb}_{0.40})_{45}\text{Zr}_{50}\text{Co}_5$, reporting a value ($1 \times 10^{-8} \text{ mol m}^{-1} \text{ s}^{-1} \text{ Pa}^{0.5}$) that is greater than that of the conventional Pd–Ag alloys. They also examined the durability of $(\text{Ni}_{0.60}\text{Nb}_{0.40})_{55}\text{Zr}_{40}\text{Co}_5$ and $(\text{Ni}_{0.60}\text{Nb}_{0.40})_{45}\text{Zr}_{50}\text{Co}_5$ at 573 K and found no change up to 100 h at 573 K, but above 673 K there was significant decay in permeation with time. Yamaura et al. [36] also reported a significant increase in hydrogen permeability in $\text{Ni}_{65}\text{Nb}_{25}\text{Zr}_{10}$, $\text{Ni}_{55}\text{Nb}_{15}\text{Zr}_{20}$, and $\text{Ni}_{60}\text{Nb}_{20}\text{Zr}_{20}$ alloys above the glass transition temperature (T_g), e.g., from 1×10^{-8} to $7 \times 10^{-8} \text{ mol m}^{-1} \text{ s}^{-1} \text{ Pa}^{-0.5}$ for $\text{Ni}_{55}\text{Nb}_{15}\text{Zr}_{20}$ at 723 K.

In order to increase the crystallization temperature, the introduction of tantalum into amorphous alloys has been explored by several groups. Kim et al. [37] compared hydrogen permeation of $\text{Ni}_{60}\text{Nb}_{30}\text{Ta}_{30}$ with $\text{Pd}_{60}\text{Cu}_{40}$ at 673 K (0.6 MPa) and reported permeabilities of 4.1×10^{-8} and $2.1 \times 10^{-8} \text{ mol m}^{-1} \text{ s}^{-1} \text{ Pa}^{-0.5}$. The next year, Hara et al. [38] reported hydrogen solution properties of $\text{Zr}_{36-x}\text{Hf}_x\text{Ni}_{64}$ ($x = 0\text{--}36$ at.%) at elevated temperatures (473–573 K) by using the Sieverts method and found that permeability increased with increasing Zr content. The equilibrium hydrogen concentration did not obey Sieverts law, however, and was nearly linear with the quarter power determined using Kirchheim theory. Hara et al. [39] established a theory of permeability as a function of hydrogen pressure and developed equations for pressure-dependent permeability from permeation tests. They also reported that the dissolution of hydrogen did not obey Sieverts' law (i.e., proportional to $P^{0.5}$). In the same year, Lee and Fleury [40] measured hydrogen permeability of $\text{Ni}_{60}\text{Nb}_{15}\text{Zr}_{10}\text{Ti}_{15}$ ($2.89 \times 10^{-8} \text{ mol m}^{-1} \text{ s}^{-1} \text{ Pa}^{-0.5}$) and $\text{Ni}_{60}\text{Nb}_{20}\text{Zr}_5\text{Ti}_{15}$ ($2.50 \times 10^{-8} \text{ mol m}^{-1} \text{ s}^{-1} \text{ Pa}^{-0.5}$) at 673–773 K and reported ~42 times larger permeability as compared to a binary $\text{Ni}_{60}\text{Nb}_{40}$ alloy membrane. Qiang et al. [41] conducted a detailed study of $\text{Ni}_{42}\text{Nb}_{28-x}\text{Zr}_{30}\text{Ta}_x$ ($x = 0, 7, 14, 21, 28$) and reported that substitution of Nb

by Ta ($\text{Ni}_{42}\text{Zr}_{30}\text{Ta}_{28}$) increased the thermal stability of the alloy. The crystallization temperatures (T_X) of $\text{Ni}_{42}\text{Zr}_{30}\text{Nb}_{28}$ and $\text{Ni}_{42}\text{Zr}_{30}\text{Ta}_{28}$ were 807 and 865 K, respectively, but although T_X increased with Ta addition, the permeability decreased.

Dolan et al. [42] reported hydrogen separation by Ni–ETM (ETM = early transition metal) amorphous membranes at the comparatively higher temperature of 673 K. They compared thermal stability and durability and hydrogen permeation of Ni-based amorphous alloys and suggested a proper balance of the eutectic alloy with an early transition metal was suitable to obtain both permeability and thermal stability. According to their thermal analysis of binary and ternary Ni–ETM eutectic alloy by non-isotherm DSC, crystallization temperature increases with addition of early transition metal as follows: $\text{Ta} > \text{Nb} > \text{Hf} > \text{Zr} > \text{Ti}$; i.e., Ta and Nb maximize thermal stability.

It is well known that Zr additions to Ni–Nb amorphous alloys lead to greater H solubility [42]; this had significant impact on the further investigation of the $\text{Ni}_{60}\text{Nb}_{40-x}\text{Zr}_x$ series for hydrogen separation applications. Dolan et al. [43] continued their studies on Ni–Zr alloys to understand the glass-forming ability of $\text{Ni}_{64}\text{Zr}_{36-x}\text{M}_x$, $x = 10$ at.% $\text{M} = \text{Ti}, \text{Nb}, \text{Mo}, \text{Hf}$ with reasonable success, but found some dimensional instabilities. The alloy ribbons with Ta and W additions produced fragmented ribbons with crystalline inclusions; thus, they became brittle and are not recommended for further studies. Thermal stability studies showed that most of the alloys exhibited T_X values in the range of 567–586 K, except for the Nb-containing alloy (602 K), which was attributed to high bond valence and slightly smaller radius of Nb. The hydrogen permeability measurement showed that $\text{Ni}_{64}\text{Zr}_{36}$ has higher permeability than $\text{Ni}_{64}\text{Zr}_{26}\text{Nb}_{10}$ and $\text{Ni}_{64}\text{Zr}_{26}\text{Ti}_{10}$ at 773 K reducing it from 2.4×10^{-9} to ca. $1.9 \times 10^{-8} \text{ mol m}^{-1} \text{ s}^{-1} \text{ Pa}^{-0.5}$. Comparing all these data concerning glass-forming ability, thermal stability, and hydrogen permeability, they concluded that the Ni–Nb–Zr system is the most important system for a hydrogen-selective membrane reactor.

4 Catalytic dissociation of hydrogen molecules by Pd and Ni coatings on non-Pd-based membranes

The suitability of Pd as a membrane material rests more with its favorable surface reaction rates than the rate of H transfer through the bulk metal. Pd is among the most active catalysts for H_2 dissociation, the essential first step in hydrogen transfer across an alloy membrane, meaning that a single layer of Pd or a Pd-based alloy can act as a H-selective membrane as its surface reaction rates are not

limiting the overall rate of H transfer across the membrane. Although Steward's [11] review shows that many metals exhibit significantly greater bulk permeability than Pd, their unfavorable surface reaction rates mean they can only function as a membrane with addition of a thin Pd catalytic overlayer coating.

This surface limitation also holds for many amorphous alloy membranes. However, Ni is known to be a highly active catalyst for H₂ dissociation [44], and Hara et al. [27] showed that amorphous Ni₆₄Zr₃₆ contains sufficient Ni to enable hydrogen permeation without need for an additional catalytic overlayer of Pd. Further examination by Spit et al. [20] and Adibhatla et al. [45] found Ni segregation on the surface of the alloy that promoted this catalytic activity. Ni also has the advantage that it can also be reduced by hydrogen at normal operating temperatures, but unfortunately Ni is not resistant to sulfur dioxide, carbon monoxide, or moisture. With reduced Ni contents, oxide formation by the ETM components renders the surface inactive, necessitating application of Pd coating. In general, elements like Nb, Ta, or Zr used in these non-Pd containing membranes always have an adherent oxide film which is not readily reduced under normal operating temperatures with hydrogen [46].

The Pd overlayer can influence the thermal stability of the membrane, as interdiffusion of Pd into the Ni-based alloy ribbons was observed in our studies [47] as well as by Buxbaum and Marker [48]. This diffusion can degrade the surface activity and can lead to the formation of impermeable compounds at the interface. More details can be found in Dolan's review [18]. In 2010, Yamaura and Inoue [49] conducted an interesting study on surface coatings of Pd and Ni on amorphous Ni₄₀Nb₂₀Ta₅Zr₃₀Co₅. They sandwiched the amorphous alloy ribbon between Pd–Pd, Ni–Ni, Pd–Ni (upstream-retentate side), and Ni–Pd (downstream-permeate side) coatings, showing that the Pd-coated retentate surfaces are resistant to poisoning by contaminant gases such as H₂S and others, while on the permeate side a simple Ni coating may be used, as there is the presence of only highly pure H₂ gas. Lewis et al. [50] showed that Pd–Au coating was more resistant to H₂S contamination. Earlier studies on surface coatings of Ni conducted by Chian et al. [51] in 2005 obtained reasonable permeation rates at 653 K.

To summarize, nearly all permeation studies of amorphous Ni–Nb–Zr membranes have been undertaken on membranes with a thin Pd overlayer on each surface. However, heat treating uncoated membranes under H₂ results in precipitation of nanocrystalline Ni, and slightly larger Zr particles, which can help in catalyzing H₂ dissociation [20, 27, 45]. This activation method has been employed when measuring hydrogen absorption via the Sieverts' method and when measuring thermal

properties of hydrided alloys via differential scanning calorimetry.

5 Crystallization in Ni–Nb–Zr alloy membranes

As indicated in Sect. 3, an important consideration for amorphous alloy membranes is thermal stability; the metastable amorphous state must be maintained during sustained operation at elevated temperature. Thermal stability can be quantified through the glass transition (T_g) and crystallization (T_X) temperatures, as well as by the activation energy of crystallization, which can be measured using the approach of Kissinger [52] and Ozawa [53]. Many studies have been performed over the years to measure these parameters, and there is a clear trend of refractory elements increasing T_g and T_X . Several studies have been performed on these alloys for different types of membranes [29, 36, 41]. We examined [54] the phase transformation and crystallization kinetics of amorphous Ni₆₀Nb₂₀Zr₂₀, finding that the activation energies for crystallization using Johnson–Mehl–Avrami (JMA) and Kissinger and Ozawa equations of 500 and 490 kJ mol⁻¹, respectively. The Avrami exponent of 2.92–2.47 indicated a diffusion-controlled three-dimensional growth mechanism of a single crystalline phase whose structure matched that of a Ni₁₀Zr₇ alloy.

In 2010, Jayalakshmi et al. [55] studied the Ni–Nb–Zr–Ta alloys of two compositions and performed X-ray diffraction, mechanical tests, and permeation studies. Further to this, Jayalakshmi et al. [56] explored the corrosion properties of amorphous Ni₆₀Nb₄₀ with alloying of Zr, Ta, Co. They found that these alloys have excellent embrittlement resistance at H/M = 0.8 and also comparable permeability to that of Ni–Nb with Pd–Cu alloy in the range 557–773 K. They also suggested that Ni–Nb-based amorphous alloy membranes could be used as bipolar plates for a proton exchange membrane fuel cell (PEMFC) due to its excellent corrosion resistance and passive current density. This is a potential new application for a material that has been studied almost exclusively for its magnetic and hydrogen permeation properties.

It is generally agreed that Nb has a beneficial effect on the mechanical stability of amorphous Ni–Nb–Zr alloys. We believe that the toughness of the material is controlled by Ni and Nb, but Zr contributes to the solubility of hydrogen in the alloy ribbon. It appears that cobalt additions also reduce the brittleness of the membrane. There are sufficient studies related to the crystallization temperatures of these amorphous membranes. Alloying additions of Ta, Hf, Nb, and Ti do improve the thermal stability and increase the crystallization temperature, but permeabilities are not enhanced, although these

membranes have excellent corrosion properties even in the presence of hydrogen.

6 Mechanical properties

Mechanical properties are of significant importance, as membranes require sufficient strength to withstand large transmembrane pressures, and while amorphous alloys are renowned for exhibiting high strength, the absorption of hydrogen can lead to embrittlement and mechanical failure under typical operating conditions. The mechanical behavior of amorphous Ni–Nb–Zr ribbons and how they vary under practical working conditions have not been extensively investigated. In general, there is little plasticity in these ribbons, and stress–strain behavior is ceramic-like; however, the ribbons are flexible when unloaded. More importantly, we are interested in the behavior of these ribbons under load with hydrogenation to simulate permeation conditions. Jayalakshmi et al. [57] reported a significant reduction of mechanical properties in $Zr_{50}Ni_{27}Ni_{18}Co_5$ and $Ni_{59}Zr_{16}Ti_{13}Nb_7Sn_3Si_2$ amorphous alloys upon hydrogenation, observing no structural and mechanical change at up to ~ 16 at.% H, but rapid crystallization was observed above 16 at.% H.

Paglieri et al. [47] examined $Ni_{40}Nb_{20}Zr_{20}$, $(Ni_{0.60}Nb_{0.40})_{100-x}Zr_x$, and $(Ni_{0.60}Nb_{0.40}Ta_{0.1})_{100-x}Zr_x$ ($x = 0$ –30 at.%) alloys, finding that hydrogen solubility and permeability increased, while the fracture resistance decreased with increasing Zr content. Ta addition decreased hydrogen permeability relative to the equivalent Ta-free alloys, but also increased the thermal stability. The alloys examined experienced a significant decrease in permeability, reducing by a factor of 2–4 over 24 h at 723 K, suggesting a structural change over time.

More recently, Zhao et al. [58] used a nanoindentation method to investigate the influence of dissolved H on shear yield strength and shear transformation zone volume of $Ni_{45}Nb_{30}Zr_{25}$, $Ni_{33}Nb_{22}Zr_{40}Co_5$, $Ni_{27}Nb_{18}Zr_{50}Co_5$, and $Ni_{35}Nb_{30}Zr_{15}Ti_{10}Fe_5Co_5$. The observations were not consistent across all alloys, with the shear yield strength increasing and shear transformation zone volume decreasing in the Zr-rich alloys ($Ni_{33}Nb_{22}Zr_{40}Co_5$ and $Ni_{27}Nb_{18}Zr_{50}Co_5$), while the opposite effect was observed in the Zr-poor alloys ($Ni_{45}Nb_{30}Zr_{25}$ and $Ni_{35}Nb_{30}Zr_{15}Ti_{10}Fe_5Co_5$). Zhao et al. [59] also observed softening in Zr-poor alloys, attributed to the mobile hydrogen in the membrane. In the Zr-rich alloys, H absorption led to hardening as H became trapped inside Zr sites, resulting in a densely packed structure.

Palumbo et al. [60] dynamic mechanical spectroscopy study of $(Ni_{0.60}Nb_{0.40})_{100-x}Zr_x$ ($x = 20$ and 30 at.%) membranes found that the elastic modulus changed sharply

between 445 and 525 K for $x = 20$ at.% and 423–473 K for $x = 30$ at.%, suggesting an amorphous to amorphous phase transition as a function of temperature. The modulus of hydrogenated membranes strongly indicated that nano-sized Zr hydrides form and dissolve as a function of temperature, and therefore, the elastic properties of the amorphous materials display a dramatic variation around these temperatures.

7 Local atomic order in the Ni–Nb–Zr alloy membranes

The absence of any structural features or long-range ordering presents a major hurdle for a full understanding of amorphous alloys and limits the effectiveness of traditional techniques such as microscopy or diffraction. Hydrogen permeation through the bulk of the alloy membranes are controlled by five important parameters, namely hydrogen solubility, hydrogen diffusivity, atomic arrangement in the membrane, probable location of hydrogen in the membrane, and mobile and trapped hydrogen sites. The first two parameters can be easily measured; the problem is the difficulty in determining the rest of the parameters in the amorphous materials. Recent work aimed at understanding short-range atomic ordering has greatly enhanced our understanding of these materials.

Yamaura et al. [61], Sakurai et al. [62], Oji et al. [63, 64], Fukuhara et al. [65], Matsuura et al. [66], and Fujima et al. [67] performed X-ray studies including RDF, EXAFS, XANES, and molecular dynamic calculations which made significant contributions toward understanding the local atomic order of these alloy membranes. They determined coordination number, arrangement of atoms in the coordination polyhedra, and interatomic distances between atoms. More studies were performed using first-principles molecular dynamics calculations; thus, the Japanese group made significant advances in understanding the nature of amorphous Ni–Nb–Zr by applying the above techniques. The local atomic structure of $(Ni_{0.60}Nb_{0.40})_{100-x}Zr_x$ ($x = 0$ –50 at.%) melt spun ribbons by XRD/RDF analyses was reported by Yamaura et al. [61]. X-ray diffraction analyses showed that the amorphous hump shifted to a lower angle with increasing Zr content that led to an increase in average interatomic distances [36]. Hydrogenation of $(Ni_{0.60}Nb_{0.40})_{70}Zr_{30}$ and $(Ni_{0.60}Nb_{0.40})_{50}Zr_{50}$ increases Zr–Zr interatomic distances, thus allowing faster hydrogen permeation.

In 2009, Palumbo et al. [60, 61] and Yamaura et al. [61] studied the effect of dissolved H on the local atomic configuration of $Ni_{42}Nb_{28}Zr_{30}$ by XAFS and showed that the local structure around Ni, Nb, and Zr atoms does not change upon H absorption. However, hydrogen charging at

higher Zr content, $\text{Ni}_{36}\text{Nb}_{24}\text{Zr}_{40}\text{H}_{11}$, alters the local structure by elongating Zr–Zr, Zr–Nb, and Nb–Ni interatomic distances. They also reported that $\text{Ni}_{36}\text{Nb}_{24}\text{Zr}_{40}$ has a distorted, 13 atom- $\text{Ni}_6\text{Zr}_6\text{Nb}$ or $\text{Ni}_5\text{Nb}_3\text{Zr}_5$ -type icosahedral structure. Based on their XAFS results, Oji et al. concluded that the $\text{Ni}_5\text{Nb}_3\text{Zr}_5$ cluster is more favorable than other polyhedral structures. Oji et al. also concluded that for the $\text{Ni}_{42}\text{Nb}_{28}\text{Zr}_{30}$ ternary alloy, H atom sites are only outside of the icosahedral cluster, and in $\text{Ni}_{36}\text{Nb}_{24}\text{Zr}_{40}$ alloy hydrogen sites, H occupies sites both outside and inside of the cluster.

A tetrahedral hydrogen occupancy site with three Zr atoms and one Nb atom is reported as a favorable configuration. In 2010, Fukuhara et al. [65] reported more refined icosahedral cluster structures of Ni–Nb–Zr–H glassy alloys by using first-principles molecular dynamics calculations and XANES measurements. Oji et al.'s [63, 64] observation of distorted icosahedral $\text{Ni}_5\text{Zr}_5\text{Nb}_3$ clusters, in which the hydrogen sites are outside the cluster in $\text{Ni}_{42}\text{Nb}_{28}\text{Zr}_{30}$, were confirmed by Fukuhara et al. [65]. In the case of $\text{Ni}_{36}\text{Nb}_{24}\text{Zr}_{40}$ alloys, H occupies tetrahedral sites surrounded by Zr, Nb, and Ni atom clusters, causing an increase in the bond distances of Zr–Zr/Zr–Nb and Nb–Ni. Matsuura et al. [66] reported on the local atomic structural effects by hydrogenation of the $(\text{Ni}_{0.60}\text{Nb}_{0.40})_{65}\text{Zr}_{35}$ ribbon to form amorphous $[(\text{Ni}_{0.60}\text{Nb}_{0.40})_{65}\text{Zr}_{35}]_{92.2}\text{H}_{7.8}$ by XAFS and molecular dynamics calculations and showed that H occupies tetrahedral sites of large icosahedra without significantly changing the local structure or coulombic oscillation. Their first-principles calculation showed that the amorphous alloy contained Ni-centered Nb triangles and formed distorted icosahedral $\text{Ni}_5\text{Nb}_3\text{Zr}_5$ clusters.

In 2013, Fujima et al. [67], using an established $\text{Ni}_5\text{Nb}_3\text{Zr}_5$ icosahedral cluster model, constructed a 112-atom rhombohedral cell structure of amorphous $\text{Ni}_{36}\text{Nb}_{24}\text{Zr}_{40}$. They suggested that Nb and Ni played very important roles in restricting crystallization and maintaining the amorphous structure. According to their calculation, the icosahedral local structure was well maintained in the amorphous phase and upon crystallization forms cuboctahedra.

Tokunaga et al. [68] employed thermodynamic modeling using CALPHAD methodology to determine the glass-forming compositional region in the ternary Ni–Nb–Zr phase diagram; results were somewhat comparable with experimental results, but an order of magnitude lower than the experimentally observed range. Density functional theory (DFT) calculations were reported as a reliable method for predictions of amorphous membranes for hydrogen permeation and purification by Hao and Sholl [69]. They performed DFT calculations on $\text{Zr}_{36}\text{Ni}_{64}$ and $(\text{Ni}_{0.6}\text{Nb}_{0.4})_{70}\text{Zr}_{30}$ and found that the experimental results of Hara et al. [27] and Ding et al. [46] were in reasonable

agreement with their calculations, but the experimental permeabilities were reported as 2–4 times smaller than those calculated.

The Ni–Nb–Zr alloys have versatile and useful material properties. For example, in addition to their excellent permeation properties, they offer interesting electrical transport properties. Fukuhara and Inoue [70, 71] and Fukuhara et al. [70–72] reported, for the first time, semi-conductivity, good electronic transport at room temperature, superconductivity, electron avalanche, and electric current coulomb oscillation in ternary $(\text{Ni}_{0.60}\text{Nb}_{0.40})_{100-x}\text{Zr}_x$ ($x = 30$ – 50) alloys with hydrogen. Fukuhara et al. [72, 73] focused on measuring the electrical resistivities of $\text{Ni}_{36}\text{Nb}_{24}\text{Zr}_{40}$ and hydrogenated $(\text{Ni}_{0.36}\text{Nb}_{0.24}\text{Zr}_{0.4})_{90}\text{H}_{10}$ alloys from 1.5 to 300 K. Experiments performed by decreasing temperatures from 300 K revealed a sudden decrease in resistivity at 6 K and found superconductive (Type II) behavior at 2.1 K. They postulated the effects of the localization of hydrogen inside and in the vicinities of the icosahedral $\text{Ni}_5\text{Nb}_3\text{Zr}_5$ clusters that may have an impact on the properties.

Chandra et al. [74, 75] performed atom probe tomography (APT) of $(\text{Ni}_{0.60}\text{Nb}_{0.40})_{100-x}\text{Zr}_x$ ($x = 0$ – 30 at.%) and revealed the coexistence of three major amorphous phases: *Phase I* (Ni-rich, considered as the matrix in the alloy), *Phase II* (Nb-rich), and *Phase III* (Zr-rich). We examined the sample $\text{Ni}_{42}\text{Nb}_{28}\text{Zr}_{30}$ by using APT and found inhomogeneity in the amorphous phase of the membrane. The overall composition of the alloy is $\text{Ni}_{42}\text{Nb}_{28}\text{Zr}_{30}$, but during the glassy ribbon formation, we found Nb-rich clusters that have a composition of $\text{Ni}_{31.78}\text{Nb}_{46.5}\text{Zr}_{21.2}$ and Zr-rich rich clusters of $\text{Ni}_{38.64}\text{Nb}_{17.9}\text{Zr}_{43.45}$, which are significantly different than the overall composition of the alloy. To illustrate this, an APT 3D-construction and proximity concentration profile on a nanoscale of the $\text{Ni}_{42}\text{Nb}_{28}\text{Zr}_{30}$ alloy in a $113 \times 109 \times 99 \text{ nm}^3$ region show all the atoms of Ni, Nb, and Zr superimposed as dots (Fig. 2a). In Fig. 2b, only Nb-enriched atom clusters are shown whose average composition is $\text{Ni}_{31.78}\text{Nb}_{46.5}\text{Zr}_{21.2}$, omitting all other Ni and Zr atoms for clarity. An area at the bottom of Fig. 2b was selected for a line scan on this small area, as shown in the inset. A proxigram concentration profile was created, averaging over all Nb-enriched clusters, as schematically shown in the inset for one cluster. The proxigram (concentration vs. distance) shows the composition variation of the $^{93}\text{Nb}^+$ and $^{58}\text{Ni}^+$ isotopes detected using the mass spectrometer across a small line of $\sim 10 \text{ nm}$ extending from point A to C. The point B shows the interface at zero mark, i.e., at the interface of the particle “C” and the matrix. As the scan approaches the interface, the Nb concentration increases and that of Ni decreases. Based on the previous research [63], we propose that these clusters are of

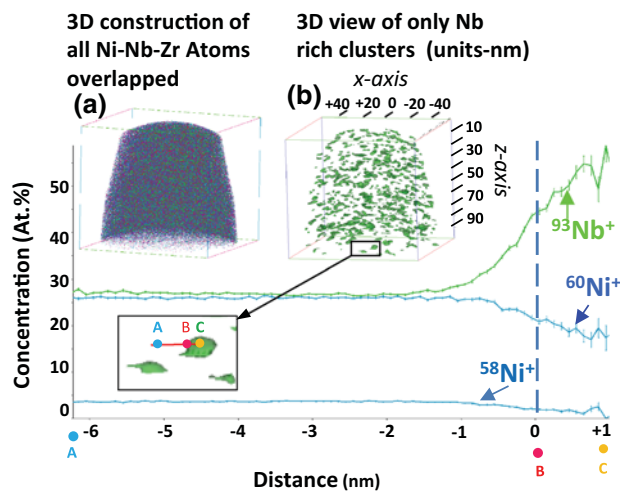


Fig. 2 **a** APT 3D-construction and proximity diagram on $\text{Ni}_{42}\text{Nb}_{28}\text{Zr}_{30}$ alloy in a $100 \text{ nm} \times 100 \text{ nm}$ cube in which all the atoms of Ni, Nb, and Zr are superimposed as *dots*. **b** Shows only the Nb-enriched clusters and excludes the Ni and Zr atoms for clarity. The average composition of the Nb-rich clusters is $\text{Ni}_{31.78}\text{Nb}_{46.5}\text{Zr}_{21.2}$ (green), different from the nominal alloy composition. A *proxigram* shows the composition variation of the $^{93}\text{Nb}^+$, $^{60}\text{Ni}^{2+}$, and $^{58}\text{Ni}^+$ isotopes

icosahedral type in these membranes. Other studies are in progress that relate to dynamic aging studies [74, 75] using neutron vibrational spectroscopy (NVS) and X-ray correlation spectroscopy (XPCS).

This review illustrates that our understanding of local atomic order in amorphous Ni–Nb–Zr alloys is advancing, but the positioning of hydrogen atoms inside the icosahedra and their vicinity needs to be explored further. Neutron vibrational spectroscopy is one tool, which may provide useful information about the hydrogen positions in icosahedra clusters of these membranes.

8 Summary

Melt spun hydrogen-selective non-precious metal amorphous alloy membranes, such as $(\text{Ni}_{60}\text{Nb}_{40})_{100-x}\text{Zr}_x$ ($x = 0, 50 \text{ at.}\%$) alloys, are emerging materials for H_2/CO_2 separation that are of industrial importance. Little was known until the last two decades or so, about the physical, local atomic order, mechanical, permeation, and electrical properties of these membranes. The research was driven by the high cost of existing Pd alloy membranes. We assembled the data from various studies and found that the permeabilities of these alloys vary by three orders of magnitude, from 1×10^{-10} to $5 \times 10^{-8} \text{ mol m}^{-1} \text{ s}^{-1} \text{ Pa}^{-0.5}$ with high hydrogen permeability between 473 and 673 K, the highest of which are comparable to those of Pd and Pd alloys. To gain a greater understanding of local ordering that will assist in the development of highly permeable, durable alloy membranes,

we performed atom tomography that revealed Nb-rich and Zr-rich amorphous clusters embedded in majority Ni matrix, whose compositions deviated from the nominal composition of the membrane. More studies on lattice dynamics such as neutron vibrational spectroscopy and X-ray correlation spectroscopy (XPCS) are in progress. More recently, Fukuhara et al. [72, 73] measured electrical properties and reported exciting new findings on semiconducting behavior at room temperature and superconducting behavior at very low temperatures. Based on all the above-mentioned studies, these alloys are not only useful for hydrogen permeation but may also contribute in electronic industrial applications.

Acknowledgments This research is supported by US DOE-NNSA Grant (US DE-NA0002004).

References

1. N.E. Amadeo, M.A. Laborde, *Int. J. Hydrogen Energy* **20**(12), 949–956 (1995)
2. S.-M. Kim, D. Chandra, N. Pal, M. Dolan, W.-M. Chien, J. Lamb, S. Paglieri, T. Flanagan, *Int. J. Hydrogen Energy* **37**, 3904–3913 (2012)
3. C. Nishimura, M. Komaki, S. Hwang, M. Amano, *J. Alloys Compd.* **330–332**, 902–906 (2002)
4. H. Hoang, H. Tong, F. Gielens, H. Jansen, M. Elwenspoek, *Mater. Lett.* **58**, 525–528 (2004)
5. M. Nishikawa, S. Shiraishi, Y. Kawamura, T. Takeishi, *J. Nucl. Sci. Technol.* **T33**, 740–780 (1996)
6. Y. Guo, G. Lu, Y. Wang, R. Wang, *Sep. Purif. Technol.* **32**, 271–279 (2003)
7. K. Yamakawa, M. Ege, B. Ludescher, M. Hirscher, H. Kronmuller, *J. Alloys Compd.* **321**, 17–23 (2001)
8. K. Yamakawa, M. Egeb, M. Hirscher, B. Ludescher, H. Kronmuller, *J. Alloys Compd.* **393**, 5–10 (2005)
9. K. Yamakawa, M. Egeb, B. Ludescher, M. Hirscher, *J. Alloys Compd.* **352**, 57–59 (2003)
10. S. Paglieri, J.D. Way, *Sep. Purif. Methods* **31**, 1–169 (2002)
11. S.A. Steward, Review of hydrogen isotope permeability through metals. US National Laboratory Report, 1983:UCRL-53441
12. W. Klement, R.H. Willens, P. Duwez, *Nature* **187**, 869 (1960)
13. A. Inoue, T. Zhang, T. Masumoto, *Mater. Trans., JIM* **33**, 965 (1989)
14. A. Inoue, *Acta Mater.* **48**, 279 (2000)
15. M. Baricco, M. Palumbo, Special issue-bulk metallic glasses. *Adv. Eng. Mater.* **9**(6), 454–467 (2007)
16. J.W. Phair, R. Donelson, *Ind. Eng. Chem. Res.* **45**, 5657–5674 (2006)
17. J.W. Phair, S.P.S. Badwal, *Sci. Technol. Adv. Mater.* **7**, 792–805 (2006)
18. M.D. Dolan, N.C. Dave, A.Y. Ilyushechkin, L.D. Morpeth, K.G. McLennan, *J. Membr. Sci.* **285**, 30–55 (2006)
19. N.W. Ockwig, T.M. Nenoff, *Chem. Rev.* **107**, 4078–4110 (2007)
20. F.H.M. Spit, J.W. Drijver, W.C. Turkenburg, S. Radelaar, G. Bambakidis (eds.), *Metal Hydrides* (Plenum, New York, 1981), pp. 345–360
21. K. Aoki, A. Horata, T. Masumoto, in *Proceedings of the 4th International Conference on Rapidly Quenched Metals 1649* (1981)
22. R.W. Lin, H.H. Johnson, *J. Non-Cryst. Solids* **51**, 45–56 (1983)

23. G. Adachi, H. Nagai, J. Shiokawa, *J. Less Common Met.* **149**, 185–191 (1989)
24. J.O. Ström-Olsen, Y. Zhao, D.H. Ryan, Y. Huai, R.W. Cochrane, *J. Less Common Met.* **172–174**, 922–92728 (1991)
25. O. Yoshinari, R. Kirchheim, *J. Less Common Met.* **172–174**, 890–898 (1991)
26. S.L.I. Chan, C.I. Chiang, *J. Alloys Compd.* **253–254**, 370–373 (1997)
27. S. Hara, K. Sakaki, N. Itoh, H.-M. Kimura, K. Asami, A. Inoue, *J. Membr. Sci.* **164**, 289–294 (2000)
28. H. Kimura, A. Inoue, S.-I. Yamaura, K. Sasamori, M. Nishida, Y. Shimpo, H. Okouchi, *Mater. Trans., JIM* **44**, 1167–1171 (2003)
29. S.-I. Yamaura, Y. Shimpo, H. Okouchi, M. Nishida, O. Kajita, H. Kimura, A. Inoue, *Mater. Trans., JIM* **44**, 1885–1890 (2003)
30. S. Hara, N. Hatakeyama, N. Itoh, H.-M. Kimura, A. Inoue, *Desalination* **144**, 115–120 (2002)
31. S. Hara, N. Hatakeyama, N. Itoh, H.-M. Kimura, A. Inoue, *J. Membr. Sci.* **211**, 149–156 (2003)
32. S.-I. Yamaura, Y. Shimpo, H. Okouchi, M. Nishida, O. Kajita, A. Inoue, *Mater. Trans., JIM* **45**, 330–333 (2004)
33. S.-I. Yamaura, S. Nakata, H. Kimura, Y. Shimpo, M. Nishida, A. Inoue, *Mater. Trans.* **46**(8), 1768–1770 (2005)
34. K. Ishikawa, T. Takano, T. Matsuda, K. Aoki, *Appl. Phys. Lett.* **87**, 081906 (2005)
35. Y. Shimpo, S.-I. Yamaura, M. Nishida, H. Kimura, A. Inoue, *J. Membr. Sci.* **286**, 170–173 (2006)
36. S.-I. Yamaura, S. Nakata, H. Kimura, A. Inoue, *Mater. Trans., JIM* **47**, 2991–2996 (2006)
37. K.B. Kim, K.D. Kim, D.Y. Lee, Y.C. Kim, E. Fleury, D.H. Kim, *Mater. Sci. Eng., A* **449–451**, 934–936 (2007)
38. S. Hara, H.-X. Huang, M. Ishitsuka, M. Mukaida, K. Haraya, N. Itoh, K. Kita, K. Kato, *J. Alloy. Compd.* **458**, 307–312 (2008)
39. S. Hara, M. Ishitsuka, H. Suda, M. Mukaida, K. Haraya, *J. Phys. Chem. B* **113**, 9795–9801 (2009)
40. D.-Y. Lee, E. Fleury, *Met. Mater. Int.* **14**, 545–548 (2008)
41. J.B. Qiang, W. Zhang, S. Yamaura, A. Inoue, *Mater. Trans., JIM* **50**, 1236–1239 (2009)
42. M.D. Dolan, N.C. Dave, L.D. Morpeth, R. Donelson, D. Liang, M.E. Kellam, S. Song, *J. Membr. Sci.* **326**, 549–555 (2009)
43. M.D. Dolan, S. Hara, N.C. Dave, K. Haraya, M. Ishitsuka, K. Kita, K.G. McLennan, L.D. Morpeth, M. Mukaida, *Sep. Purif. Technol.* **65**, 298–304 (2009)
44. D.M. Viano, M.D. Dolan, F. Weiss, A. Adibhatla, *J. Membr. Sci.* **487**, 83–89 (2015)
45. A. Adibhatla, M.D. Dolan, W. Chien, D. Chandra, *J. Membr. Sci.* **463**, 190–195 (2014)
46. H.Y. Ding, W. Zhang, S.I. Yamaura, K.F. Yao, *Mater. Trans., JIM* **54**, 1330–1334 (2013)
47. S. Paglieri, N. Pal, M. Dolan, S. Kim, W. Chien, *J. Membr. Sci.* **378**, 42–50 (2011)
48. R.E. Buxbaum, T.L. Marker, *J. Membr. Sci.* **85**, 29–38 (1993)
49. S.-I. Yamaura, A. Inoue, *J. Membr. Sci.* **349**, 138–144 (2010)
50. A.E. Lewis, H. Zhao, H. Syed, C.A. Wolden, J.D. Way, *J. Membr. Sci.* **465**, 167–176 (2014)
51. W.C. Chian, W.D. Yeh, J.K. Wu, *Mater. Lett.* **59**, 2542–2544 (2005)
52. H.E. Kissinger, *Anal. Chem.* **29**, 1702 (1957)
53. T. Ozawa, *J. Therm. Anal.* **2**, 301 (1970)
54. S.-M. Kim, W.-M. Chien, D. Chandra, N.K. Pal, A. Talekar, J. Lamb, M.D. Dolan, S.N. Paglieri, T.B. Flanagan, *J. Non-Cryst. Solids* **358**, 1165–1170 (2012)
55. S. Jayalakshmi, Y.G. Choi, Y.C. Kim, Y.B. Kim, E. Fleury, *Intermetallics* **18**, 1988–1993 (2010)
56. S. Jayalakshmi, V.S. Vasantha, E. Fleury, M. Gupta, *Appl. Energy* **90**, 94–99 (2012)
57. S. Jayalakshmi, S.O. Park, K.B. Kima, E. Fleury, D.H. Kim, *Mat. Sci. Eng. A* **449–451**, 920–923 (2007)
58. Y. Zhao, I.-C. Choi, M.-Y. Seok, U. Ramamurty, J. Suh, J.-I. Jang, *Scr. Mater.* **93**, 56–59 (2014)
59. Y. Zhao, I.-C. Choi, M.-Y. Seok, M.-H. Kim, D.-H. Kim, U. Ramamurty, J. Suh, J.-I. Jang, *Acta Mater.* **78**, 213–221 (2014)
60. O. Palumbo, S. Brutti, F. Trequattrini, S. Sarker, M. Dolan, D. Chandra, A. Paolone, *Energies* **8**, 3944–3954 (2015). doi:10.3390/en8053944
61. S.-I. Yamaura, M. Sakurai, M. Hasegawa, K. Wakoh, *Acta Mater.* **53**, 3703–3711 (2005)
62. M. Sakurai, S. Yamaura, K. Wakoh, E. Matsubara, A. Inoue, *J. Metastable Nanocryst. Mater.* **24–25**, 551–554 (2005)
63. H. Oji, K. Handa, J. Ide, T. Honma, N. Umesaki, S. Yamaura, M. Fukuhara, A. Inoue, S. Emura, *J. Phys. Conf. Series* **190**, 012075-1 (2009)
64. H. Oji, K. Handa, J. Ide, T. Honma, S. Yamaura, A. Inoue, N. Umesaki, *J. Appl. Phys.* **105**, 113527-1 (2010)
65. M. Fukuhara, N. Fujima, H. Oji, A. Inoue, S. Emura, *J. Alloys Compd.* **497**, 182–187 (2010)
66. M. Matsuura, M. Fukuhara, K. Konno, T. Fujita, M.W. Chen, N. Fujima, A. Inoue, *J. Non-Cryst. Solids* **357**, 3357–3360 (2011)
67. N. Fujima, T. Hoshino, M. Fukuhara, *J. Appl. Phys.* **114**, 063501-1 (2013)
68. T. Tokunaga, S. Matsumoto, H. Ohtani, M. Haesebe, *Mater. Trans., JIM* **48**, 2263–2271 (2007)
69. S. Hao, D.S. Sholl, *J. Membr. Sci.* **350**, 402–409 (2010)
70. M. Fukuhara, A. Inoue, *Phys. B* **405**, 3630–3632 (2010)
71. M. Fukuhara, A. Inoue, *J. Appl. Phys.* **105**, 063715 (2009)
72. M. Fukuhara, H. Yoshida, K. Koyama, A. Inoue, Y. Miura, *J. Appl. Phys.* **107**, 033701–033705 (2010)
73. M. Fukuhara, H. Yoshida, A. Inoue, N. Fujima, *Intermetallic* **80**, 1864–1866 (2010)
74. D. Chandra, Behavior of Ni–Nb–Zr alloy gas permeation membrane ribbons at extreme pressure condition, 2014 Yearly Report on US DOE Contract No. DE-NA0002004 May 13, (2014)
75. D. Chandra, Behavior of Ni–Nb–Zr alloy gas permeation membrane ribbons at extreme pressure condition, 2015 Yearly Report on USDOE Contract No. DE-NA0002004 August 18, (2015)